Available online at www.eccomasproceedia.org
Eccomas Proceedia COMPDYN (2023) 5288-5299

ECCOMAS
Proceedia

COMPDYN 2023
9th ECCOMAS Thematic Conference on
Computational Methods in Structural Dynamics and Earthquake Engineering
M. Papadrakakis, M. Fragiadakis (eds.)
Athens, Greece, 12-14 June 2023

PERFORMANCE EVALUATION OF A MASONRY ARCH BRIDGE UNDER COMBINED SCOUR AND TRAFFIC LOADING

Prateek K. Dhir[1*], Daniele Losanno[2], Fabrizio Scozzese[3], Enrico Tubaldi[4], and Fulvio Parisi[5]

[1*] Department of Structures for Engineering and Architecture, University of Naples Federico II, Italy.
e-mail: prateek.dhir@strath.ac.uk

[2] Department of Structures for Engineering and Architecture, University of Naples Federico II, Italy.
e-mail: daniele.losanno@unina.it

[3] School of Architecture and Design, University of Camerino, Italy.
e-mail: fabrizio.scozzese@unicam.it

[4] Department of Civil and Environmental Engineering, University of Strathclyde, Glasgow, UK.
e-mail: enrico.tubaldi@strath.ac.uk

[5] Department of Structures for Engineering and Architecture, University of Naples Federico II, Italy.
e-mail: fulvio.parisi@unina.it

Abstract

Masonry arch bridges are highly vulnerable to floods - particularly to scour - due to their stiff and relatively fragile behavior, combined with the fact that they are often built on shallow foundations. In multi-span masonry arch bridges interaction of structural members give rise to a complex response when subjected to scour action combined with traffic loading.
The present work evaluates the behavior of a case study scoured masonry bridge under traffic loading with a three-dimensional finite element model developed in Abaqus using a macro-modelling approach. Traffic load model is selected in accordance with a recent guideline for safety assessment of existing bridges in Italy. The scouring process is then imposed through the progressive removal of elements from the model at the foundation. Displacement and internal stress distribution is analyzed under combined action due to increasing traffic load and scour depth.
The outcomes of the research lay the basis for an accurate risk assessment and management of masonry arch bridges subjected to multiple hazards. The proposed study can also provide useful information in terms of thresholds levels for bridge monitoring and maintenance.

Keywords: Flood risk assessment, Masonry arch bridges, Floods, Scour, Traffic loading, multi-hazard, Macro-model.

ISSN:2623-3347 Published by Eccomas Proceedia.
Peer-review under responsibility of the organizing committee of COMPDYN 2023.
doi: 10.7712/120123.10800.21274

1 INTRODUCTION

Masonry bridges are always vulnerable to scour and scour-induced settlements, due to their existing shallow footings. Due to the high population of existing masonry-arch bridges in Europe and worldwide [1] and their socio-economic, cultural, and historical value, the accurate assessment of their capacity against scour is of primary concern.

Only few numerical studies have addressed this issue by considering complex soil-foundation-structure interaction models [2,3]. These studies have investigated the significance of accurately accounting for the geometry of the scour hole when determining the bridge's capability against scour and the mechanism of collapse. Due to the differences in both the geometry and the pattern of the loading, it is not possible to precisely characterise the complicated behavior of these structural systems without using numerical three-dimensional (3D) models. Aiming at describing the progression of the cracking mechanism in the masonry components, improved models have been suggested in recent years (see e.g., [2, 4, 5]).

The performance of scoured masonry bridges under combined traffic loading moving from the case of the Rubbianello bridge is investigated in this study. In this regard, a 3D finite element model is developed in Abaqus software with a macro-modelling approach. While explicitly neglecting soil-foundation interaction, the scouring process is described by the progressive removal of constraints at the foundation level of the model. The outcome of the study facilitates the evaluation of residual capacity to traffic loads while increasing scour depth at the base and provide useful information for future bridge monitoring and maintenance.

2 CASE STUDY

The 1906-built stone arch bridge spans over the Aso river in the Central Italian town of Rubbianello. However, a very severe flood in 2013 was responsible for the collapse of two of the seven spans due to the flood induced scour. Again, earthquakes in 2016 as well as the severe rains and flooding until 2017 led to the present condition of the bridge (3 piers and 3 bays) (Figure 1). In this study the remaining bridge portion are modelled by introducing a new artificial abutment on the right side (in place of the existing pier) to obtain a symmetric configuration of the sample bridge.

Figure 1: Rubbianello bridge at its present condition [6]: (a) top-view and (b) lateral view.

2.1 Bridge geometric details

The original 7-span bridge has a span length of 16 m. Piers are identical and each of size 9.5 m × 3.2 m. Arches were 0.95m thick with a radius of 11.58 m. Spandrel walls of 0.65 m thickness were built. The foundations under the piers were rectangular in plan (11.00 m × 3.90 m) with a depth of 4.15 m. Figure 2 shows more information on the bridge geometry showing the original length (Figure 2a) and transverse (Figure 2b) and longitudinal (Figure 2c) section of the bridge.

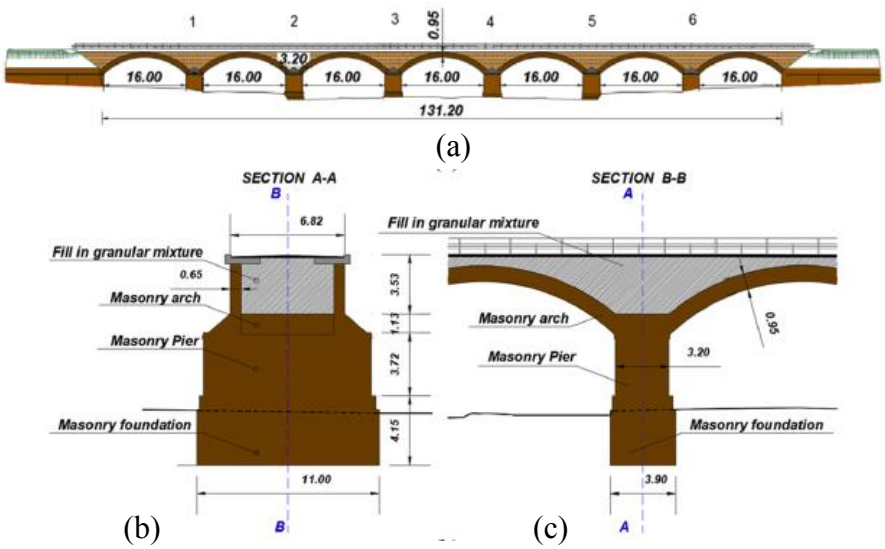

Figure 2: Geometrical details showing; (a) original length, (b) transversal, and (c) longitudinal. (Units are in meters) [6].

2.2 Materials

The selected material mechanical properties for the present analysis are taken from Scozzese et al. [6]. The material properties assigned to the abutment and the backfill were selected from the literature [2, 4, 5]. The summary of the major mechanical strength parameters presented in Table 1, i.e. density (ρ), Young's modulus (E), peak compressive strength ($f_{y,c}$), and peak tensile strength ($f_{y,t}$).

Material	ρ [t/m^3]	E [kN/m^2]	$f_{y,c}$ [kN/m^2]	$f_{y,t}$ [kN/m^2]
Masonry (Arches & Spandrels)	1.80	3,100,000	2,000	150
Masonry (Piers)	1.75	2,900,000	2,000	150
Backfill	1.70	250,000	10	0
Abutment	1.90	300,000	-	-

Table 1: Main mechanical properties [6].

3 NUMERICAL MODEL

A finite element 3D model was developed using Abaqus 2018 [7] platform, considering both geometrical and mechanical nonlinearities. Continuum (solid) elements are used with C3D8R (8-node linear, reduced integration, hourglass control). To obtain a balance between the computational cost and accuracy, the mesh dimensions are kept in the range between 0.35 m and 0.75 m as per [5, 6]. The material nonlinearity is described by concrete damage plasticity (CDP) model already available in Abaqus [7]. The material flow parameters for the CDP model presented in Table 2 are obtained from [6]. A linear elastic model is employed with a Mohr-Coulomb failure criterion (55° friction angle and 10 kN/m^2 cohesion) for the backfill material.

Nonlinear frictional/cohesive interfaces [2, 3] are used to simulate the interactions between the two components (arch-to-pier, spandrel-to-pier, spandrel-to-arch, and masonry-mortar interfaces) of the bridge. These zero thickness interfaces represent the mortar joints present at the

interaction between the parts. A damage criterion is introduced for masonry-mortar interfaces (see Table 3) whose properties are taken from [2, 5].

dilation angle	flow potential eccentricity	$\frac{f_{b0}}{f_{c0}}$	K	Viscosity parameter
31^0	0.1	1.16	0.67	0.001

Table 2: flow parameters governing the CDP model.

Interaction Properties	Backfill-masonry	mortar
Coefficient of friction, μ (-)	0.6	1.0
K_n per unit area (N/mm^3)	500000	500000
K_t, K_s per unit area (N/mm^3)	500000	500000
σ_t (kN/m^2)	-	150
Cohesion, c (kN/m^2)	-	210
Normal fracture energy per unit area, G_f^I (kN/m)	-	0.05
Shear fracture energy per unit area, G_f^{II} (kN/m)	-	0.1

Table 3: Properties of the contact interfaces.

4 TRAFFIC LOAD ANALYSIS

Traffic load is a random variable to be modelled in safety assessment of roadway bridges. To model realistic traffic actions applied to existing bridges, recently developed traffic-load models (TLMs) proposed in [8] are considered in this study. Three load vehicles were considered in terms of spacing and single axles distribution to be representative of heavy (5-axles), medium (3-axles) and light (2-axles) real traffic, respectively (Figure 3). In addition to concentrated loads, uniform load was applied outside the silhouette of the single vehicle for the whole length of the bridge.

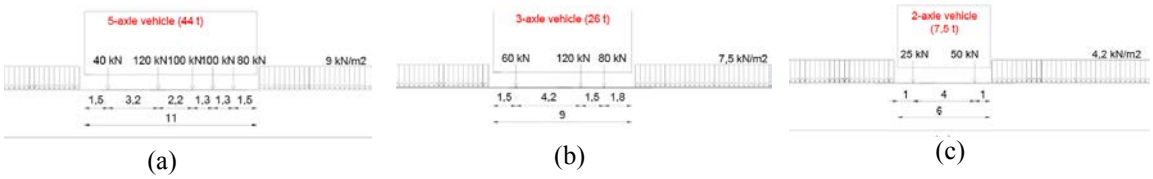

(a) (b) (c)

Figure 3: New traffic load models (distance in m): (a) heavy (5-axles), (b) medium (3-axles), (c) light (2-axles) vehicle [8].

A parametric study was conducted to examine stresses and displacements developed at various sections of the bridge with varying TLMs imposed on a single lane on the downstream side. Figure 4 identifies the critical sections under consideration where $F_{1,2}$ refers to the foundations, $P_{1,2}$ refers the piers, $A_{1,2}$ and $B_{1,2}$ refers to the arches and the backfills connecting P_1, respectively.

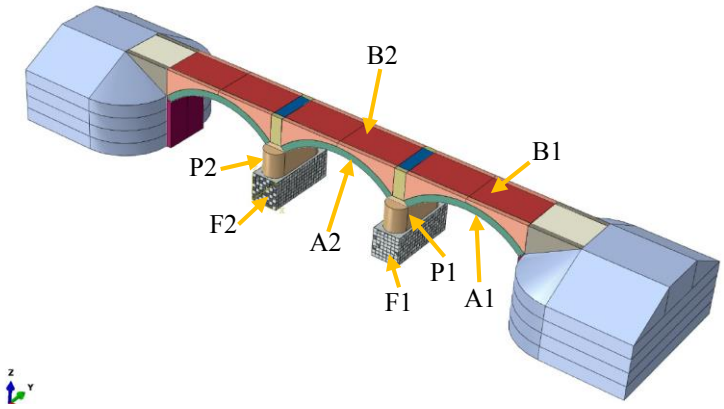

Figure 4: Numerical model showing the sections under considerations for stress analysis.

Figure 5a shows a comparison of displacements recorded at the bottom of the pier (P1) for the selected TLMs. After imposing gravity loads (i.e., Step-0), traffic loads were assigned (i.e., Step-1). Figure 5b and Figure 5c shows peak compressive stress and peak tensile stress, attained at selected sections of the bridge. As expected, the highest stresses and displacements are seen for 5-axle followed by 3-axle and 2-axle TLM. The highest stresses are observed in the arches and the lowest in the backfills.

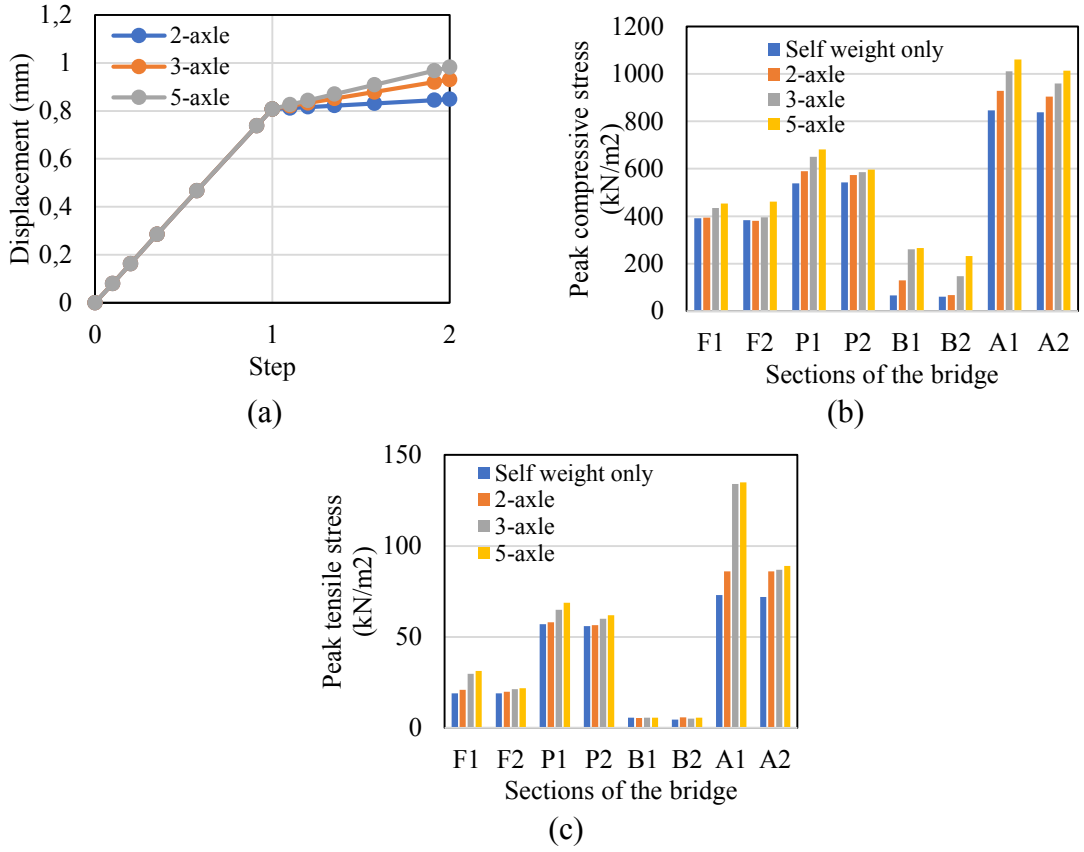

Figure 5: (a) Comparisons of displacements recorded at P1 (b) peak compressive stress (c) peak tensile stress under varying heavy TLM.

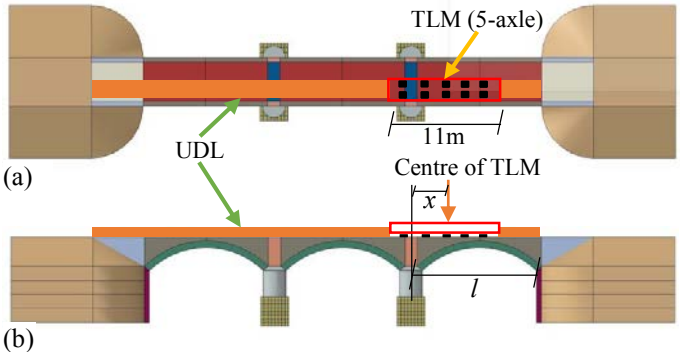

Figure 6: (a) top view and (b) side view of the bridge showing the loading schemes of heavy TLM.

A simplified influence line study was also conducted to assess the influence of moving traffic load axles along the span length, *l* of the bridge. Four models are developed for heavy TLM (5-axles). In the first case, the heavy TLM is applied being the centre of the TLM lying on the top of the P1 (i.e., x=0). Similarly, in the other three models, the TLM is applied at a length of $x=l/4$, $x=l/2$, and $x=3l/4$ from the center of P1. Figure 6 presents a schematic diagram showing top and side view of the bridge with TLM scheme.

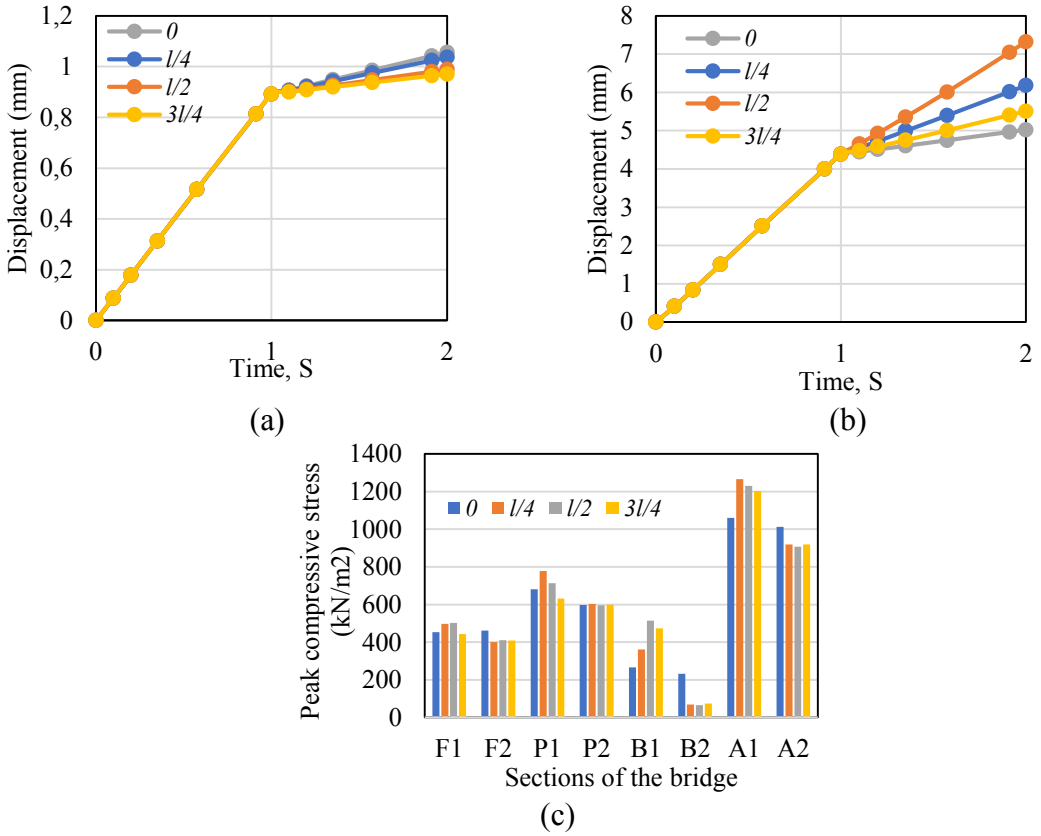

Figure 7: Comparisons of displacements recorded at (a) P1 (b) A1, and (c) stresses of 5-axle of traffic loading under varying positions.

Figure 7a shows a comparison of the displacements recorded at the pier top under gravity and traffic loading. The highest displacement is recorded at P1 when the TLM is acting at a distance x=0. As we move the TLM towards the crown the displacement recorded at P1 reduces and the least displacement at the pier top (P1) is observed when the traffic load is

at $x=3l/4$. Similarly, the highest displacement in the crown at A1 is observed (Figure 7b) when the center of TLM is close to the crown of A1 (i.e., $x=l/2$), and the least is when the $x=0$. Figure 7c shows the peak compressive stresses developed at the various sections of the bridge for the examined positions.

5 COMBINED SCOUR AND TRAFFIC LOAD ANALYSIS

Scour is a natural phenomenon caused by the erosion or removal of streambed or bank material from bridge foundations due to flowing water [2, 8-10]. The progression of scour is numerically simulated by removing support conditions (i.e., releasing joints at the base) under the foundation. A total of 8 scour scenarios were modelled aiming to represent different levels of maximum scour depth (Figure 8). Step 1 corresponds to the starting condition with gravity and traffic loads only acting on the bridge, i.e., no scour. From Step 2 to Step 9, the scour development is simulated by considering increments of scouring depth, for a total maximum scour depth of 5.54m (50% of the total foundation length) attained at Step 9. A dimensionless parameter is introduced in terms of scour portion b over total foundation length B, i.e., b/B, varying from 0 to 0.5.

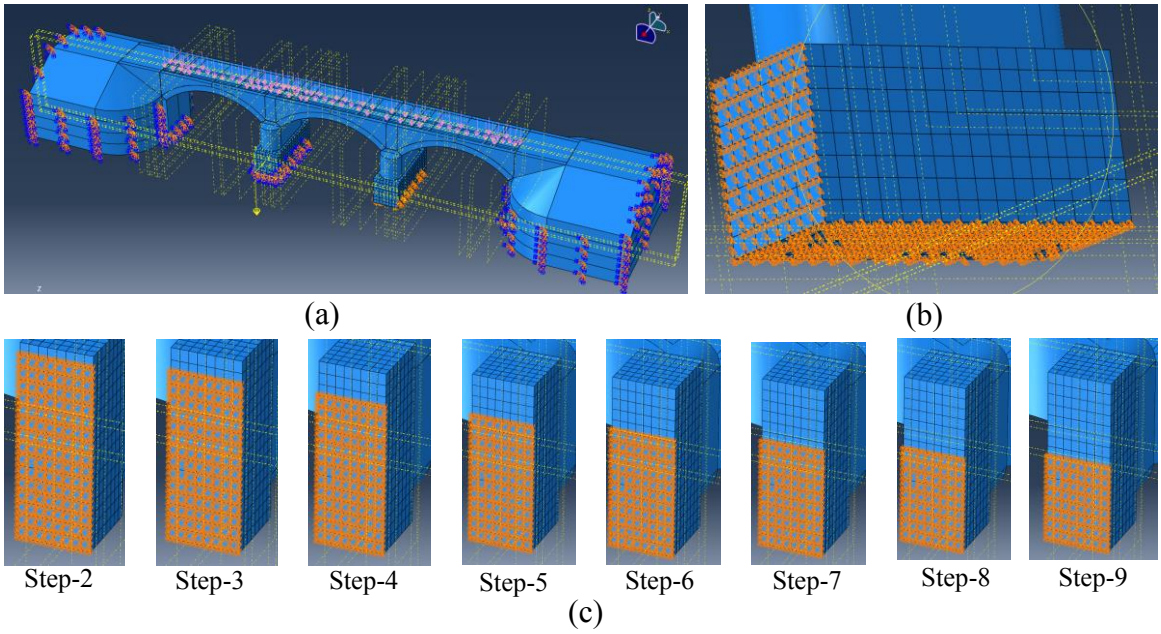

Figure 8: (a) Numerical model developed in Abaqus (a) foundation boundary conditions (c) progress of removal of supports representing settlements ($0 < b/B < 0.5$).

Figure 9 show the peak compressive stress distribution in the foundation (F1) subjected to scour under traffic loading at different steps. With gravity load only the stress distribution contours are symmetric with all axes (Step-0). With the addition of traffic loading at one of the two lanes of the road, unsymmetric stresses are developed and higher stresses are seen on the side of the foundation on which the loading is present (Step-1). To impose the most adverse condition, scouring action is simulated (from Step 2 to 9) downstream, i.e., under the same lane traffic has been applied. With the increment of scouring levels, the location of the highest stress point shifts from the edge of the foundation to its center.

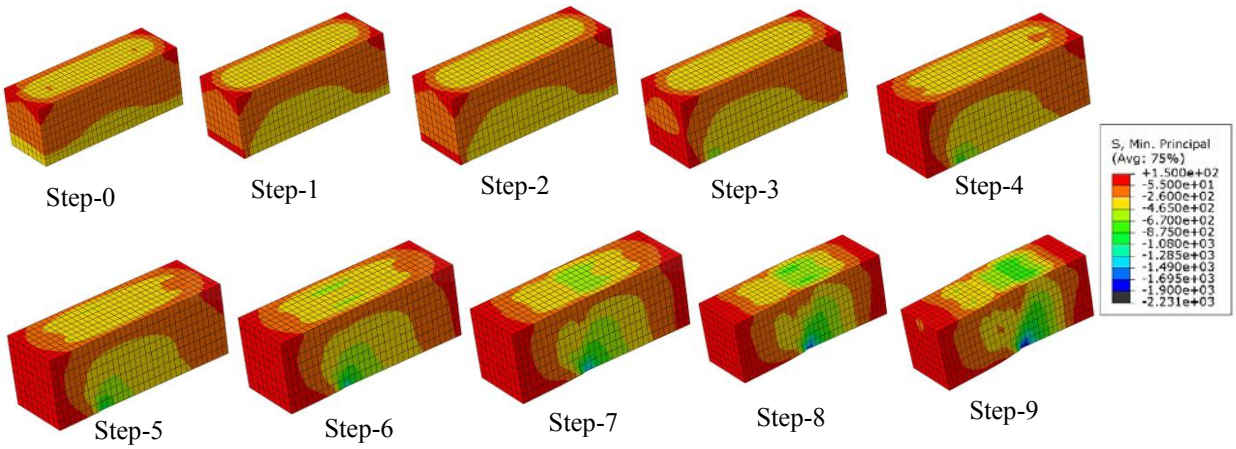

Figure 9: Foundation compressive stress distribution subjected to scour under traffic loading.

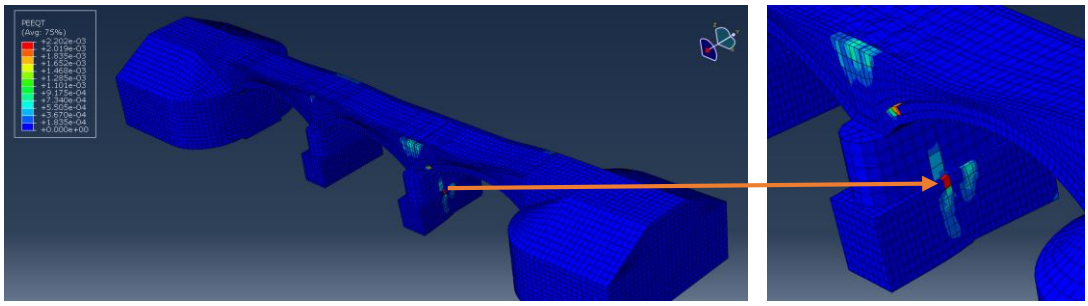

Figure 10: Equivalent plastic strain (PEEQT) distribution subjected to scour under traffic loading.

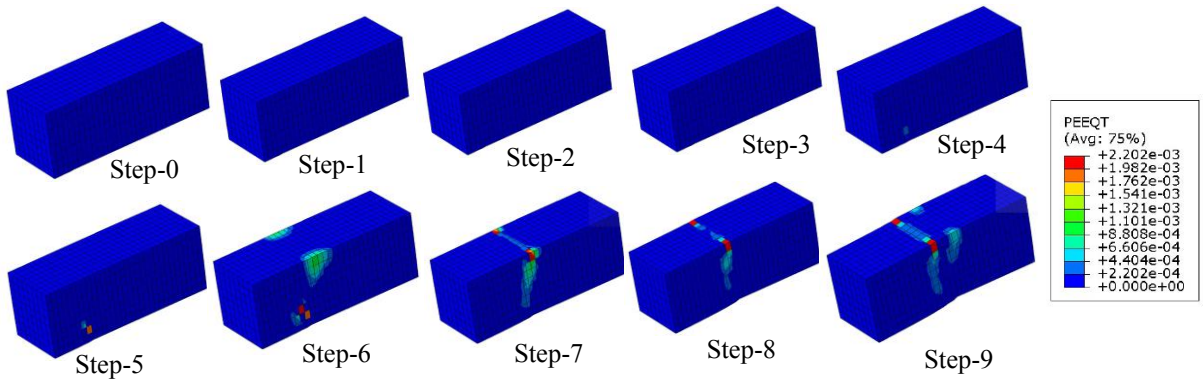

Figure 11: Equivalent plastic strain (PEEQT) distribution of the foundation subjected to scour under traffic loading.

Figure 10 shows the plastic strain distribution of the whole model at Step-9 scouring level and the progress of plastic strain in F1 for each step are presented in Figure 11. Up to Step-3 no visible strain is identified whereas from the Step-4 onwards (i.e., $b/B > 0.19$) plastic strains are developed, and stresses start concentrating at F1, which also begins rotating. Figure 12a illustrates the comparisons of the pier's vertical settlement at P1 against b/B with reference to the case where no traffic load is considered. For an increasing heavy TLM intensity by a load multiplier (LM) of 2.5 and 5, the comparisons are shown in Figure 12b, c and finally all the cases are compared in Figure 12d. The vertical settlement notably increases for increasing value of

b/B. When the *b/B* reaches 0.3, further small increments induce a very high increase in stresses causing damage to the structure.

Figures 13a shows the peak compressive stress distribution for all critical sections of the bridge subjected to scour only where no traffic load is imposed. Figure 13b shows the condition where a 5-axle TLM is applied and propagated up to 8th scouring level (step-9). In Figure 13c and 12d, traffic load multipliers of 2.5 and 5 were applied and the responses are compared with respect to the condition where scouring occurs without any application of traffic loading. Similarly, Figure 14 shows the peak tensile stresses developed with increasing traffic load factors.

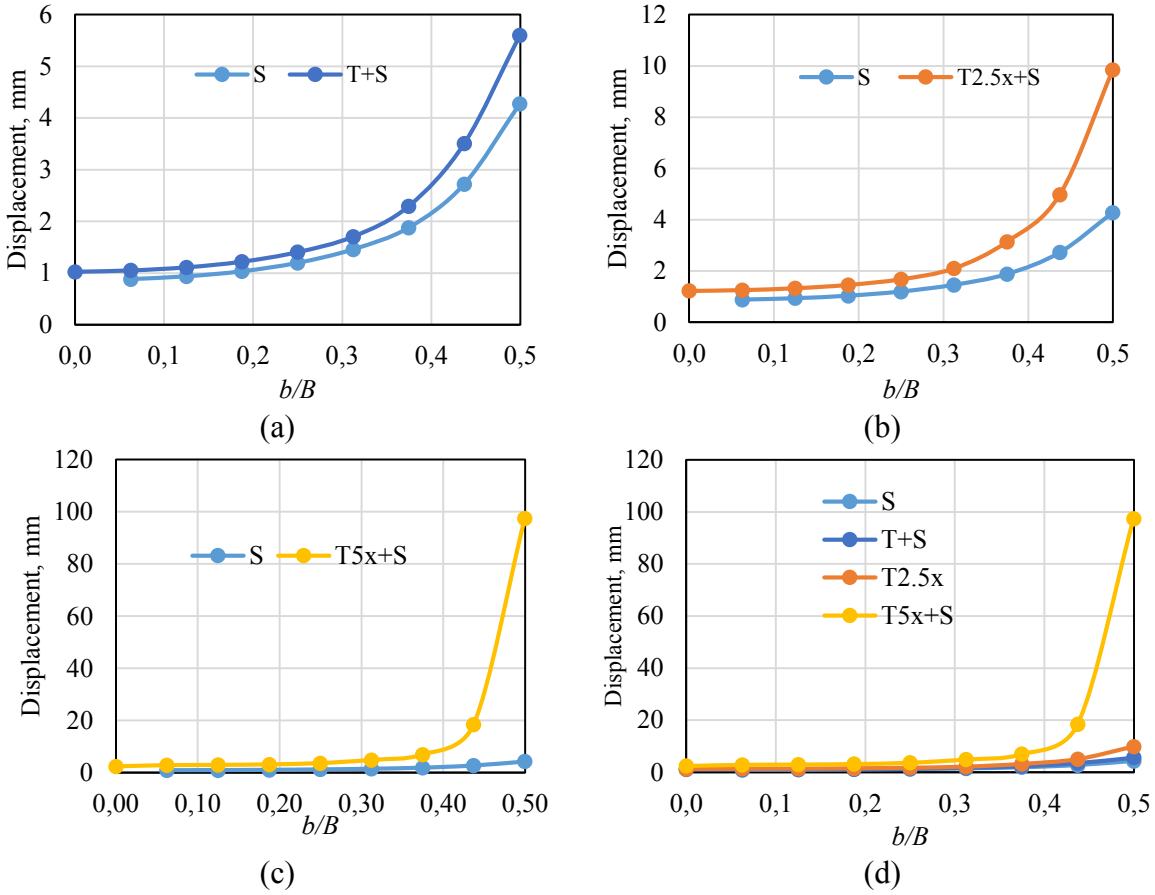

Figure 12: Displacement at foundation subjected to scour under heavy TLM: (a) T+S (b)2.5T+S, (c) (5T+S) and (d) all cases.

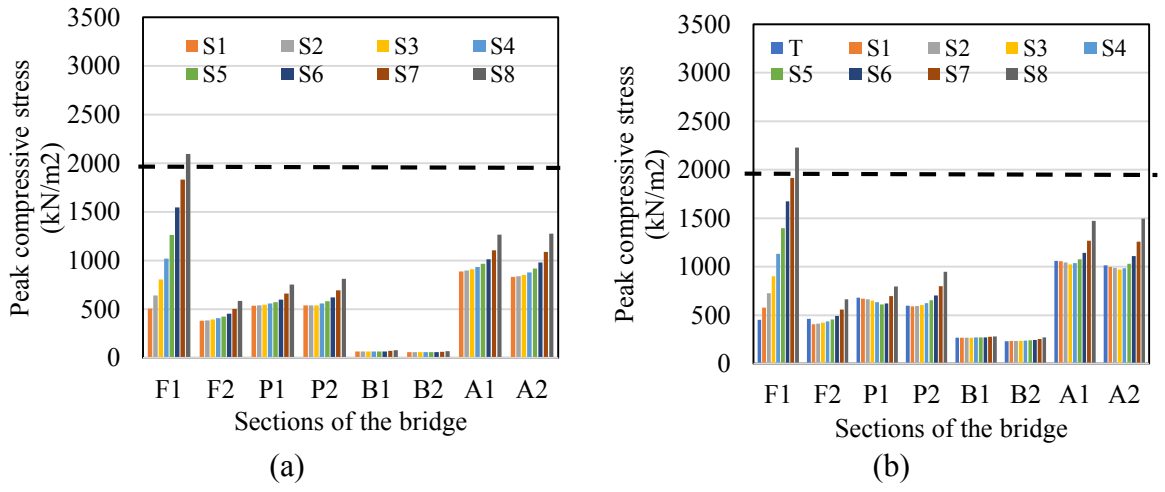

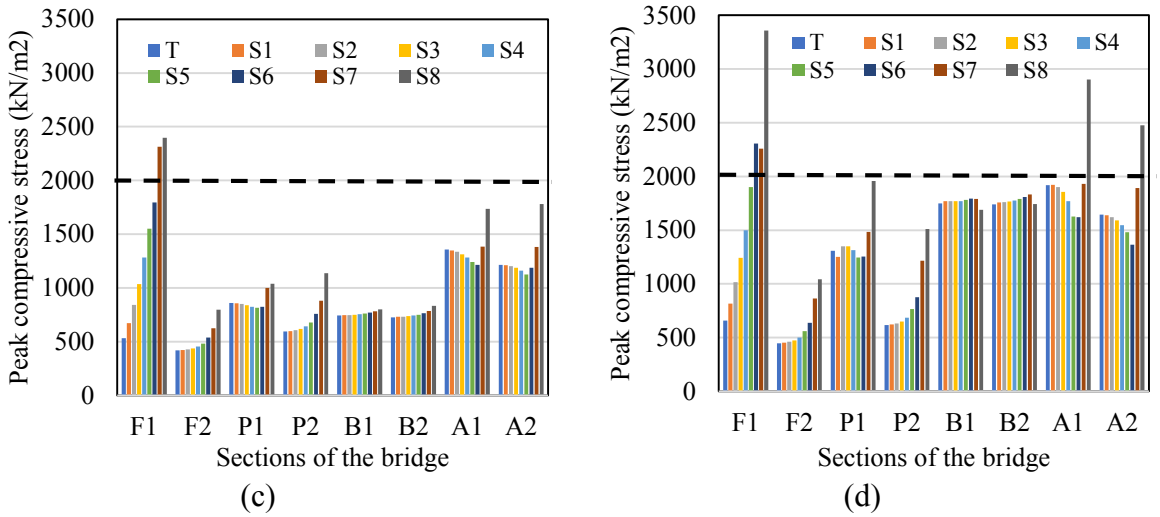

Figure 13: Peak compressive stress under combined heavy TLM and scour: (a) T+S (b)2.5T+S, (c) (5T+S) and (d) all cases.

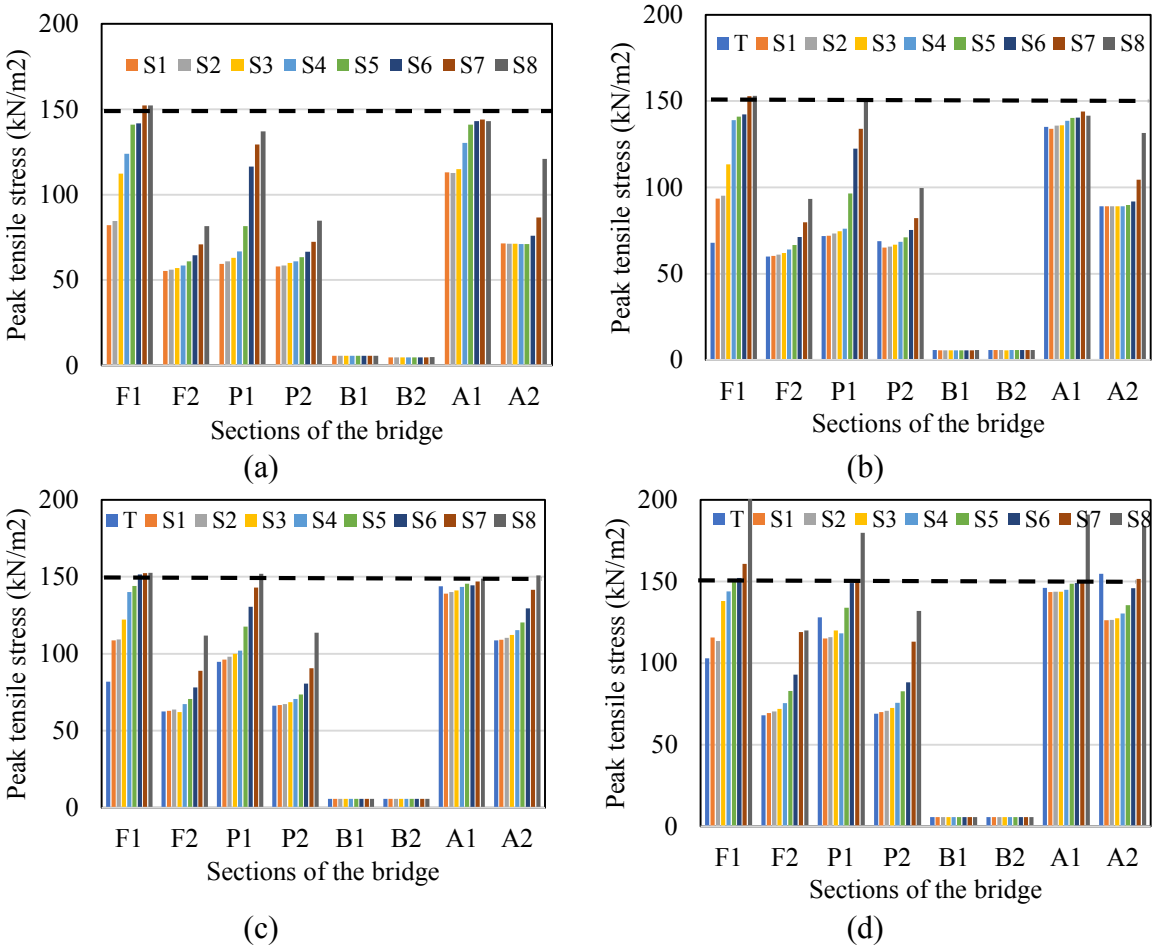

Figure 14: Peak tensile stress under combined TLM and scour: (a) T+S (b)2.5T+S, (c) (5T+S) and (d) all cases.

Figure 15a shows the comparison of stresses developed at F1 for all selected steps (Step 1-9) with an increasing TLM factor of 1, 2.5 and 5. Higher compressive stresses are developed with the progress of scouring level which is consistent with increasing traffic load factors. Figure 15b shows a comparison of compressive stress Demand to Capacity ratios (DCR) of the

section F1 against *b/B*. Once the *b/B* reaches 0.3 the DCR rises sharply leading to the failure confirming previous outcomes in terms of plastic strain and vertical displacement.

Similarly, the development of tensile stress recorded for F1 is shown in Figure 15c with an increasing level of traffic load factors. The tensile stress approaches the capacity limit (150 kN/m^2) once it completes the Step-3. It increases further with the increase in the scouring levels and Step-5 onward it attains the maximum limit leading to the failure. Figure 15d shows a comparison of tensile DCRs for the section F1 where DCR reaches to 1 at *b/B*>0.3. DCRs provide a useful representation in terms of interaction domain between traffic loads and scour depth accounting for reduced bridge residual safety due to mutual action.

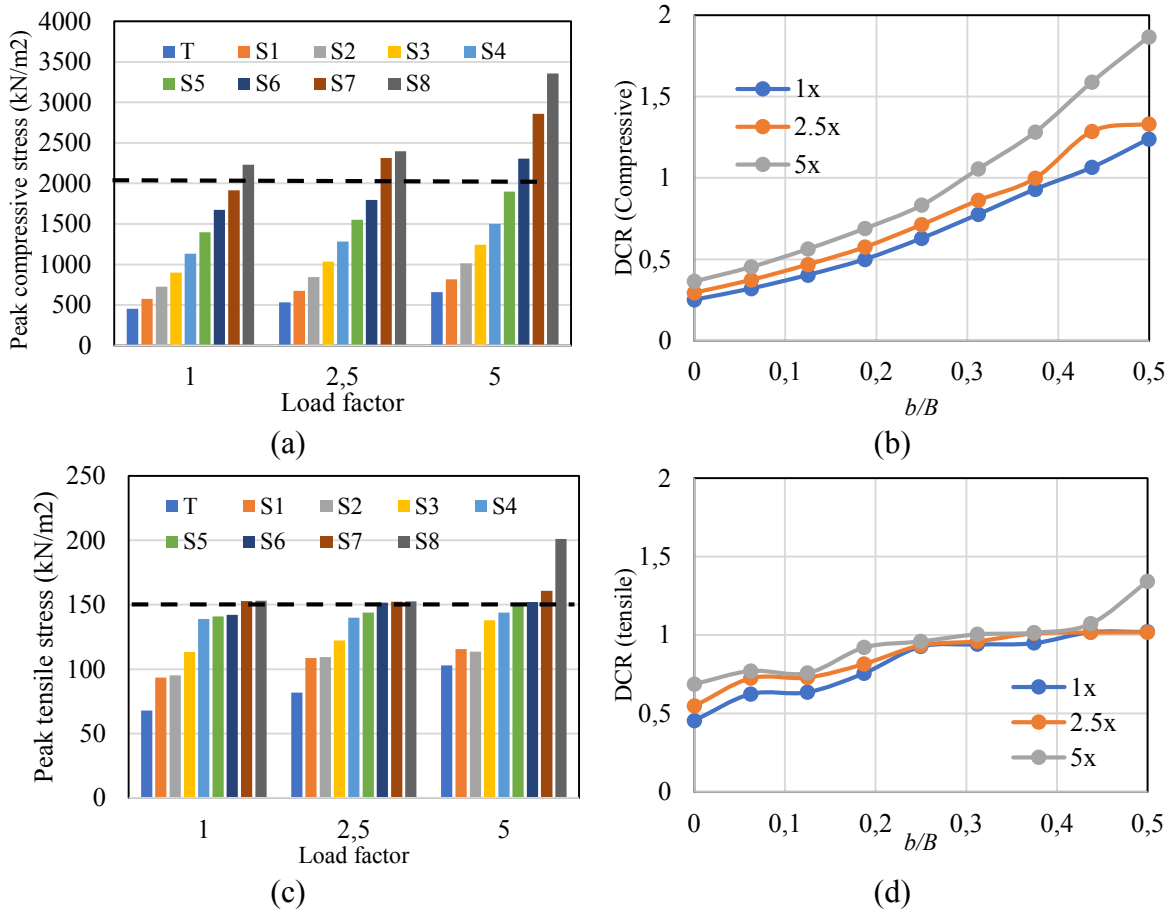

Figure 15: (a) Peak compressive stresses (b) compressive DCR (c) Peak tensile stresses (d) tensile DCR

6 CONCLUSIONS

This study performs a performance evaluation of scoured masonry bridges under traffic loading. In the initial stage of the study, the solo influence of the traffic loading without scour as well as the scouring without any imposed traffic loading was investigated. Parametric studies were conducted considering loading types and the traffic loading locations. Later, the model was analysed for increasing levels of scour subjected to traffic loading. An increasing level of load factors for the traffic loading was also considered to combine different intensity levels of the actions.

Once the *b/B* reaches 0.3, the DCR rises sharply leading to failure. Both the compressive and the tensile stresses reach close to the capacity limit once *b/B*=0.3. DCR reaches 1 at *b/B*>0.3 as it increases further with the increase in the scouring levels leading to the failure. As far as

the scour depth increases, the safety factor against traffic loads reduces. Once the scouring length of the foundation reaches 30% of its original dimension, any contribution in terms of traffic loading may cause complete failure of the structure.

The outcome of the research facilitates the accurate risk assessment and management of masonry arch bridges subjected to combined scour and traffic action, laying the basis for future studies on multi-hazard scenario and safety assessment of existing bridges.

ACKNOWLEDGEMENT

This study was carried out in the framework of RESIST project "RobustnEss aSsessment and retrofItting of bridgeS to prevenT progressive collapse under multiple hazards", which is funded by University of Naples Federico II and Compagnia di San Paolo through STAR Plus Programme 2020. The support by ReLUIS through the CS.LL.PP.–ReLUIS programme is also gratefully acknowledged.

REFERENCES

[1] J. Page, Masonry Arch Bridges: State-of-the-art Review. *HM Stationery Office*, 1993.

[2] E. Tubaldi, L. Macorini, B. A. Izzuddin, Three-dimensional mesoscale modelling of multi-span masonry arch bridges subjected to scour." *Engineering Structures*, **165**, 486-500, 2018.

[3] P. Zampieri, M. A. Zanini, F. Faleschini, L. Hofer, C. Pellegrino, Failure analysis of masonry arch bridges subject to local pier scour. *Engineering Failure Analysis*, **79**, 371-384, 2017.

[4] Y. Zhang, E. Tubaldi, L. Macorini, B.A. Izzuddin, Mesoscale partitioned modelling of masonry bridges allowing for arch-backfill interaction. *Construction and Building Materials*, **173**, 820-842, 2018.

[5] G. Milani, P. B. Lourenço, 3D non-linear behavior of masonry arch bridges. *Computers & Structures*, **110**, 133-150, 2012.

[6] F. Scozzese, L. Ragni, E. Tubaldi, F. Gara, Modal properties variation and collapse assessment of masonry arch bridges under scour action. *Engineering Structures*, **199**,109665, 2019.

[7] S. Dassault. SIMULIA User Assistance 2018: Abaqus Verification Guide. *Dassault Systèmes Simulia Corp*, 2018.

[8] E. Cosenza, D. Losanno, Assessment of existing reinforced ‐ concrete bridges under road ‐ traffic loads according to the new Italian guidelines. *Structural Concrete*, **22 (5)**, 2868-2881, 2021.

[9] G. Hoffmans, *JCM. Scour manual*. Routledge, 2017.

[10] B. W. Melville, S. E. Coleman, Bridge scour. *Water Resources Publication*, 2000.

[11] E. Tubaldi, L. Macorini, B. A. Izzuddin, C. Manes, F. Laio, A framework for probabilistic assessment of clear-water scour around bridge piers. *Structural safety*, **69**, 11-22, 2017.